THE ASTROPHYSICAL JOURNAL, 474:735–740, 1997 January 10
© 1997. The American Astronomical Society. All rights reserved. Printed in U.S.A.

VARIATIONS IN THE 3 MICRON SPECTRUM ACROSS THE ORION BAR: POLYCYCLIC AROMATIC HYDROCARBONS AND RELATED MOLECULES

G. C. SLOAN[1] AND J. D. BREGMAN
NASA Ames Research Center, MS 245-6, Moffett Field, CA 94035-1000; sloan@ssa1.arc.nasa.gov, bregman@ssa1.arc.nasa.gov
T. R. GEBALLE
Joint Astronomy Centre, 660 N. A'ohoku Place, Hilo, HI 96720; tom@jach.hawaii.edu
L. J. ALLAMANDOLA
NASA Ames Research Center, MS 245-6, Moffett Field, CA 94035-1000; allamand@ssa1.arc.nasa.gov
AND
CHARLES E. WOODWARD[1,2]
University of Wyoming, Department of Physics and Astronomy, Laramie, WY 82071-3905; chelsea@wapiti.uwyo.edu
Received 1996 March 29; accepted 1996 August 6

ABSTRACT

Long-slit spectra across the Orion Bar reveal significant differences in the spatial behavior of the components of the 3 μm polycyclic aromatic hydrocarbon (PAH) spectrum. The strong PAH band at 3.29 μm generally decreases exponentially with distance from the ionization front into the molecular cloud (scale height $\sim 12''$), although excesses appear $\sim 10''$ and $\sim 20''$ behind the ionization front, close to layers of H_2 and CO emission, respectively. The 3.40 μm PAH feature separates into two components with very different spatial distributions. The main component (at 3.395 μm), along with the 3.51 μm band and the PAH plateau (3.3–3.6 μm), shows excess emission $\sim 10''$ and $\sim 20''$ behind the ionization front, stronger than the excesses in the 3.29 μm band. The extra component of the 3.40 μm band, which peaks at ~ 3.405 μm, has a spatial distribution very similar to the H_2 emission. Aromatic C—H stretches in PAHs most likely produce the 3.29 μm feature. Aliphatic C—H stretches in either attached methyl side-groups or superhydrogenated PAHs, or perhaps both, could produce the complicated spectral and spatial structure at 3.40 μm.

Subject headings: dust, extinction — infrared: ISM: lines and bands — ISM: individual (Orion Bar) — ISM: molecules

1. INTRODUCTION

The discovery of the unidentified infrared (UIR) emission bands in NGC 7027 and BD +30°3639 (Gillett, Forrest, & Merrill 1973; Merrill, Soifer, & Russell 1975) opened a new field in infrared astronomy. The UIR spectrum shows strong emission bands at 3.3, 6.2, 7.7, and 11.3 μm, along with several weaker components. Sellgren (1984) discovered that a 1000 K continuum often accompanied the UIR bands in reflection nebulae and proposed that this continuum resulted from fluorescence of very small particles upon the absorption of a single UV photon. Carbon-rich material is robust enough to survive the hard radiation environments in which the UIR bands originate, making polycyclic aromatic hydrocarbons (PAHs) the leading candidate (Allamandola, Tielens, & Barker 1985; Léger & Puget 1984).

Several other carriers have also been proposed, but most invoke a hydrocarbon material containing aromatic structures. The energetics require that the emitting molecules contain on the order of 20–60 carbon atoms. When one of these large molecules absorbs a UV photon, the energy is distributed over all of the vibrational modes of the molecule. The molecule relaxes by emission from C—H and C—C vibrations, producing the characteristic spectrum (Allamandola, Tielens, & Barker 1989; Léger, d'Hendecourt, & Défourneau 1989). Most models agree on the general identifications for individual bands, but some uncertainties about the exact molecular structure remain. Sakata et al. (1987) and Papoular et al. (1989) argue that the 7.7 μm band may require an oxygen component in the molecules. Several authors also suggest that a significant fraction of the carbon may be tied up in aliphatic or amorphous structures (Jones, Duley, & Williams 1990, and references therein; Borghesi, Bussoletti, & Colangeli 1987; Blanco, Bussoletti, & Colangeli 1988). For the sake of simplicity, we will simply refer to the carriers as PAHs in the discussion that follows.

This spectroscopic study focuses on the emission features in the 3 μm region that arise in large part from C—H stretching modes. In fact, the first identification of the 3.29 and 3.40 μm bands with C—H vibrations predates any of these models (Grasdalen & Joyce 1976). Overtones of C—C bands at 6.2 μm may also contribute to emission in the 3–4 μm region. In most astrophysical sources, emission in the 3.29 μm band dominates the 3–4 μm region and is usually accompanied by a weaker band at 3.40 μm along with a broad emission plateau extending out to ~ 3.6 μm (Geballe et al. 1985). In some objects, weaker features at 3.46, 3.51, and 3.56 μm also are apparent superposed on the plateau (de Muizon et al. 1986).

The Orion Bar is a region of transition between the ionized Orion Nebula (H II region) to the northwest and the neutral molecular cloud to the southeast (see Fig. 1). Such zones, described as photodissociation regions (PDRs; Tielens et al. 1993), often produce PAH emission. The Orion Bar shows a very strong and rich PAH spectrum in the 3 μm region (Geballe et al. 1989). As the distance from the ionization front into the PDR increases, the strength of

[1] Visiting Astronomer, United Kingdom Infrared Telescope.
[2] NSF Presidential Faculty Fellow.

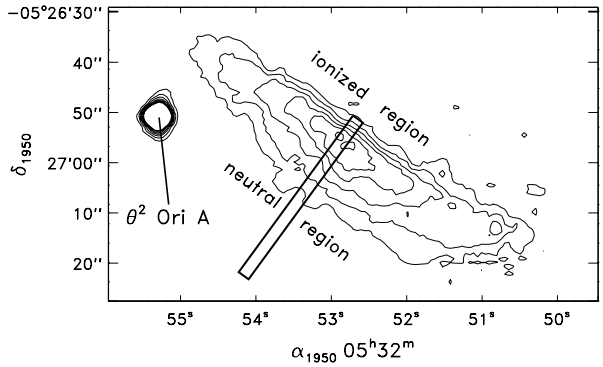

FIG. 1.—Location of the slit position within the Orion Bar emission region, presented with contours from narrowband imaging of the Bar at 3.29 μm (courtesy of Bregman & Sloan 1996). The region northwest of the Bar is fully ionized by the Trapezium, which is $\sim 2'$ from the Bar. The ionization front lies along the ridge of highest 3.29 μm emission, and the material to the southeast remains neutral.

the UV field and the ratio of far-UV to near-UV photons declines, producing several different emission layers. Atomic lines dominate in the ionized region. PAH bands peak at the ionization boundary and extend into the cloud (Bregman et al. 1989, 1994; Bregman & Sloan 1996). H_2 emission peaks further ($\sim 10''$) into the neutral region, and CO and CS emission occur even deeper in the molecular cloud ($\sim 20''$) (Tielens et al. 1993; van der Werf et al. 1996). The Orion Bar presents these layers to the observer with a favorable edge-on geometry, making the different emission regions easily distinguishable.

We have measured the spatial and spectral behavior of the 3 μm spectrum of the Orion Bar using a long-slit spectrometer. By orienting the slit perpendicular to the ionization front, we have observed how the PAH spectrum changes with increasing depth into the molecular region. This method provides constraints on the carriers of the observed bands and shows how their abundances can vary across a PDR.

2. TECHNIQUE

We observed the Orion Bar at the 3.8 m United Kingdom Infrared Telescope (UKIRT) with the 75 lines mm^{-1} grating of CGS4, the facility near-infrared long-slit spectrometer. CGS4 uses a 256 × 256 InSb detector array, but for these observations in the 3 μm window, we read out only a 32-row subarray (32 × 256). We used the short camera mirror (150 mm), resulting in each row spanning 1.″23 on the sky. Figure 1 illustrates the orientation and position of the slit on the Bar, determined by offsetting from θ^2 Ori A. We subtracted the thermal background from each spectral image by observing in a standard chop-and-nod sequence. On 1995 October 28 (UT), we observed with a 2 pixel (2.″5) slit, chopping east-west 90″, and integrating on-source for 37.3 minutes. On 1995 October 29 (UT), we used a 1 pixel (1.″2) slit, chopped east-west 94″, and integrated on-source for 40 minutes. On both nights, the wavelength coverage extended from 3.02 to 3.70 μm. The spectral resolution ($\lambda/\Delta\lambda$) after all processing was approximately 600 the first night and 1000 the second night. We modified the chop throw between nights to check for contamination from emission in the reference beams and found none. Continuum emission would not affect our results, and Sellgren (1981) did not observe any significant emission sources at 3.28 μm at the location of our reference beams.

Individual images were flatfielded at the telescope and then co-added. To correct for the slight tilt in a spectrum across the array and the slight shift in wavelength along the slit, we rectified (i.e., straightened) the co-added images using a spline-fitting algorithm. This latter step degraded both the spatial and spectral resolution slightly. We used spectra of HR 1687 (F5 V) as a standard to correct for atmospheric and instrumental transmission. We avoided the difficulty of correcting for the 3.31 μm telluric methane absorption feature by simply interpolating over this feature in all rows in our spectra. We also interpolated over some bad pixels in rows 11–12 at 3.44 μm.

Figure 2 illustrates how the spectrum changes with position in the Orion Bar region. We extracted equivalent fluxes from all of the identified spectral features from each row in each image in order to study quantitatively how the strength of the features varied with spatial position. We first removed the continuum from each row by fitting a line to the endpoints of the spectrum. To estimate the contribution from the PAH plateau, we represented it with a series of line segments fit to the spectrum at 3.210, 3.230, 3.360, 3.440, 3.490, 3.540, 3.590, and 3.610 μm (± 0.005 μm). This method presupposes that the PAH plateau is not just a combination of overlapping wings of the features we are studying, a point to which we will return below. The emission above this estimated plateau we assigned to the individual PAH and

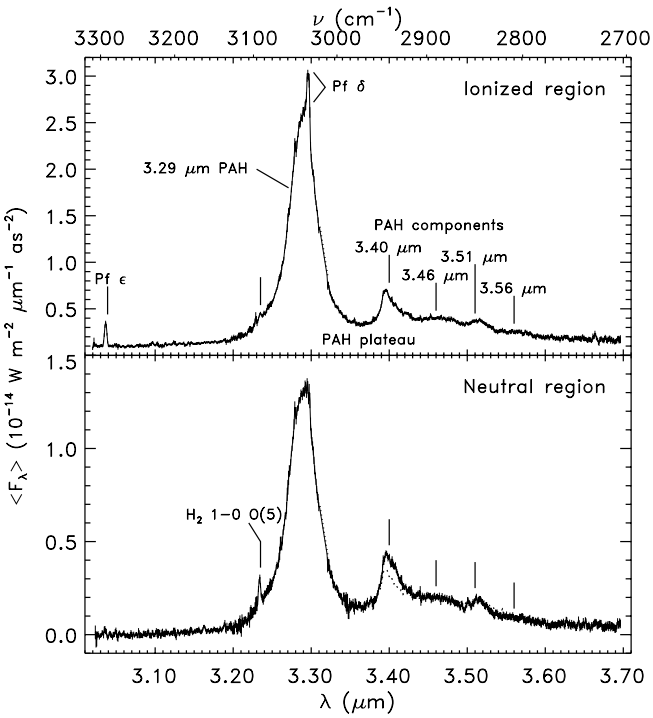

FIG. 2.—Comparison of spectra from the ionized region (*top*) and neutral region (*bottom*) of the Orion Bar. The spectrum from the ionized region is the sum of all rows up to the ionization front (rows 0–6). The spectrum from the neutral region is the sum of rows 11–15 (i.e., 7″–11″ behind the ionization front). Both spectra are taken from the night of October 29, when we were observing with a 1″ slit. From the ionized to the neutral region, the strength of the PAH feature at 3.40 μm has increased relative to the 3.29 μm band, and its shape has changed. To illustrate this, we have scaled the 3.40 μm feature from the ionized region and plotted it in the bottom panel (*dotted line*).

TABLE 1

EXTRACTION OF FLUXES OF PAH FEATURES

λ_0 (μm)	Assumed λ Range (μm)
3.29.....	3.240–3.320
3.40.....	3.380–3.435
3.46.....	3.445–3.485
3.51.....	3.495–3.535
3.56.....	3.545–3.585

hydrogen features as shown in Table 1. Finally, we subtracted the flux from the H_2 1–0 O(5) and H II Pfδ lines (where positive) from the 3.29 μm PAH band. We estimated the uncertainties by using the rms noise in the spectrum and by comparing our extractions from the two separate nights. In the plots of equivalent flux versus position below, we always plot the larger of these two estimates of the error for each data point.

3. RESULTS

The row of maximum PAH emission is located in a region of rapid change in the strength of the hydrogen recombination lines. We (somewhat arbitrarily) define this row as the ionization front. Behind this front, the PAH bands generally drop in intensity with increasing distance into the molecular region, though not all in the same manner. A key to identifying the carriers of the individual bands may lie in the differences in their spatial behavior.

Figure 3 illustrates the behavior of the atomic (H II) and molecular (H_2) hydrogen emission. The atomic lines drop exponentially from the ionized to the neutral region, with a $1/e$ scale height (d_0) of 9″. The H_2 line behaves quite differently, rising to a peak $\sim$10″ behind the ionization front and dropping in intensity further back.

All of the bands fall in intensity on either side of the ionization front (Figs. 4 and 5). Within the ionized region, this drop is thought to result from the destruction of the PAH molecules by the intense UV field (Bregman et al. 1989). Within the neutral region, the drop results from the attenuation of the UV photons exciting the PAH emission as the distance into the molecular cloud increases. The intensity of the 3.29 μm PAH band decreases with a $1/e$ scale height (d_0) of 12″, but it shows an excess over this exponential falloff $\sim$20″–26″ behind the ionization front. The PAH plateau, which emits about two-thirds of the

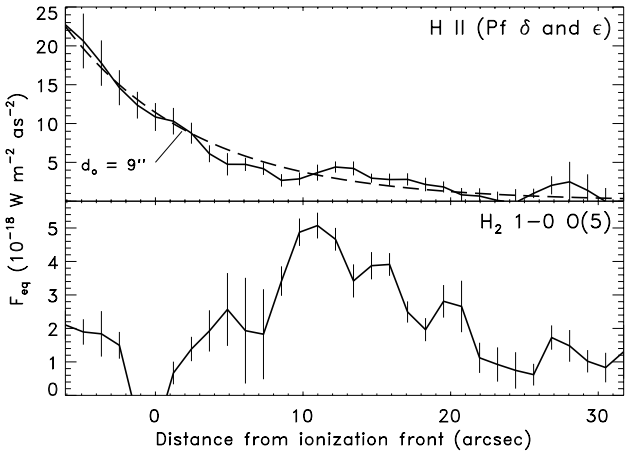

FIG. 3.—Behavior of the strengths of the hydrogen recombination (*top*) and H_2 emission (*bottom*) lines. The H II data are averaged from the Pfδ and Pfϵ lines and decrease approximately as an exponential with scale height (d_0) of 9″ (*dashed line*).

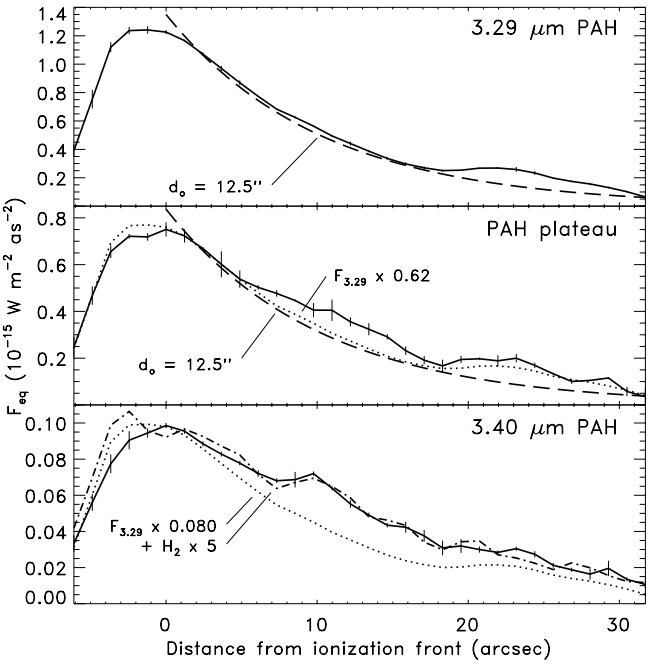

FIG. 4.—Spatial behavior of the stronger PAH emission features. *Top:* the 3.29 μm band compared to an exponential (scale height $d_0 \approx 12\farcs5$, *dashed line*). *Middle:* the PAH plateau compared to the 3.29 μm band (scaled, *dotted line*) and an exponential (*dashed line*). *Bottom:* the 3.40 μm band compared to the 3.29 μm band (scaled, *dotted line*) and a combination of the 3.29 μm and H_2 profiles (*dash-dotted line*).

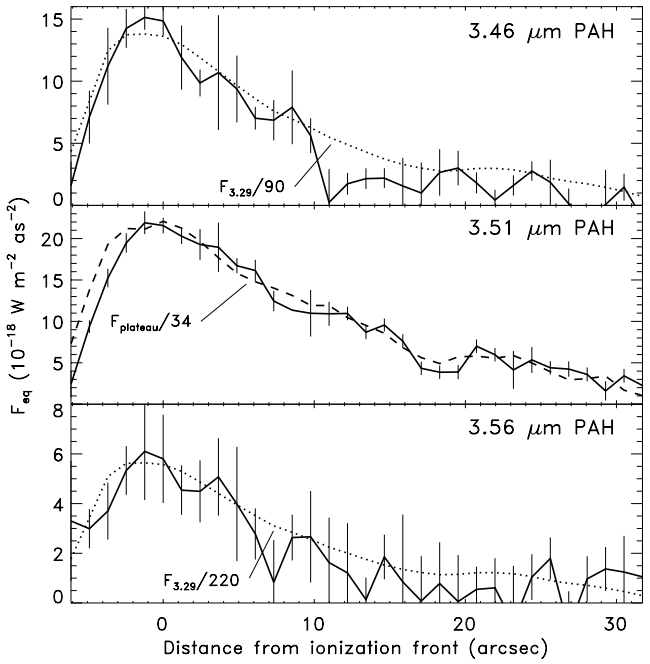

FIG. 5.—Spatial behavior of the weaker PAH emission features. *Top:* the 3.46 μm band. *Middle:* the 3.51 μm band. *Bottom:* the 3.56 μm band. The 3.29 μm band (scaled, *dotted line*) and the PAH plateau (scaled, *dashed line*) are plotted for comparison.

energy of the 3.29 μm feature, has a similar intensity distribution, although it shows a much stronger excess $\sim 10''$ behind the ionization front. The 3.40 μm PAH feature emits about 1/10 the intensity of the 3.29 μm band. The 3.40 μm excess $\sim 10''$ behind the ionization front is even stronger than the excess in the PAH plateau, showing a sharp rise from $8''$ to $10''$ behind the front. Interestingly, this excess traces the H_2 emission very closely. The 3.46 μm PAH band generally behaves as the 3.29 μm band, but drops to near zero $\sim 10''$ behind the ionization front and beyond. While the error bars indicate that this drop may not be statistically significant, it is interesting that it occurs at the position where H_2 emission peaks and the 3.40 μm band and PAH plateau show an excess. The 3.51 μm PAH band behaves in a manner very similar to the PAH plateau and the 3.40 μm feature, showing excesses $\sim 10''$ and $\sim 20''$–$25''$ behind the ionization front. We have also detected the emission feature at ~ 3.56 μm near the ionization front, but the rather large uncertainties in our extracted fluxes prevent us from drawing any conclusions other than that it exists and approximately follows the other bands.

The shape of the 3.40 μm feature changes significantly from the front of the Bar into the molecular region (Fig. 2), suggesting the existence of a second emission component with a different spatial distribution. To test this hypothesis, we averaged the shape of the feature in rows 0–5 in our spectral images (i.e., from inside the ionized region up to the ionization front), scaled this average shape to each subsequent row, subtracted it, and summed the residual intensity. Figure 6 illustrates the results. The main component of the putative 3.40 μm band actually peaks at 3.395 μm, while the extra component peaks at ~ 3.405 μm. Figure 7 compares the relative spatial distributions of these two components. The extra component closely traces the distribution of the H_2 emission.

This similarity raises the possibility that the extra component arises from an H_2 line. Two H_2 transitions occur in the 3.4 μm region: 3–2 O(5) at 3.395 μm and 0–0 S(19) at 3.404 μm. Unresolved molecular lines in our data have a FWHM of 0.003 and 0.005 μm in the $1''$ and $2''$ slits, respectively, while the extra component at 3.405 μm has a much broader FWHM of 0.014 μm. A careful examination of the bottom panel of Figure 2 reveals the marginal presence of the 3–2 O(3) 3.163 μm and 2–1 O(4) 3.189 μm lines. Based on the observed strengths of these lines compared to the 1–0 O(5) transition at 3.23 μm and predictions of fluorescence models (Black & van Dischoeck 1987), we could expect the 3–2 O(5) transition to contribute, at most, 2% of the main 3.40 μm component. This value represents an upper limit, because van der Werf et al. (1996) find that thermal excitation dominates fluorescent emission within $15''$–$20''$ of the Bar. They estimate the temperature of the H_2 to be ~ 2000 K, making the expected contribution of the 3–2 O(5) line inconsequential. At 2000 K, the contribution of the 0–0 S(19) line would be less than 1% of the extra 3.40 μm component. Therefore, on the basis of expected line strengths and widths, we conclude that neither H_2 line could account for the main or the extra component of the 3.40 μm feature.

If we assume that the PAH plateau is not a separate entity but rather an artifact produced by the overlap of the 3.40, 3.46, 3.51, and 3.56 μm PAH bands, the total flux from the 3.40 μm feature and other weak bands increases substantially. Analyzing the data from this point of view, the main component of the 3.40 μm feature and the 3.51 μm band would still follow each other closely. The bands at 3.46 and 3.56 μm would also show similar behaviors to the 3.40 and 3.51 μm bands, since the majority of their emission arises from what we would otherwise assign to the plateau, and this emission behaves similarly to the 3.40 and 3.51 μm bands. Finally, our conclusions about the extra component of the 3.40 μm feature would remain unchanged.

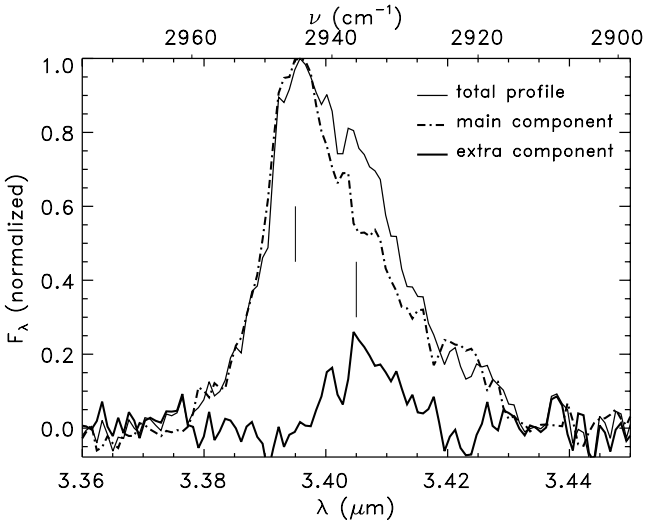

FIG. 6.—Changing shape of the 3.40 μm emission feature (from the October 29 data). *Thin solid line:* the 3.40 μm feature summed from all rows beyond $2''$ behind the ionization front. *Dash-dotted line:* the main component of the 3.40 μm feature, summed from all rows within the ionized region. *Thick solid line:* the difference of the above two curves, revealing the extra component. The two vertical lines mark the approximate peaks of the components at 3.395 μm and 3.405 μm.

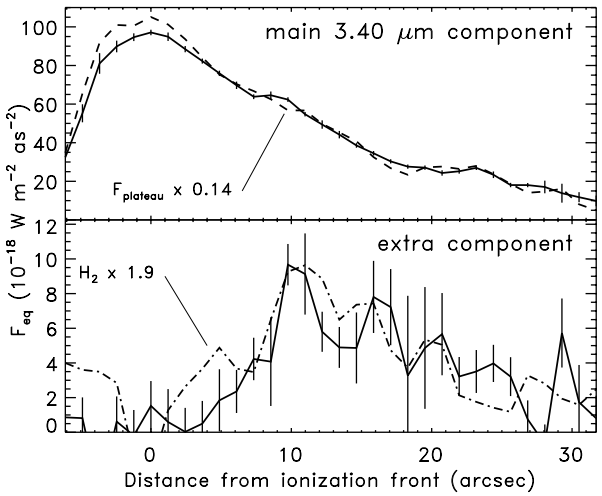

FIG. 7.—Relative spatial behavior of the two components of the 3.40 μm feature. The main component (*top*) follows the PAH plateau (*dotted line*), while the extra component (*bottom*) follows the H_2 emission (*dash-dotted line*).

4. DISCUSSION

After separating the 3.40 μm band into two components, the main component still shows an excess $\sim 10''$ behind the ionization front. The spatial behavior of the strength of this band, the PAH plateau, and the 3.51 μm band are all very

similar. In each, the excess emission $\sim 10''$ behind the ionization front is similar to the intensity distribution of the H_2 line emission. All three bands also show an additional excess $\sim 20''$ behind the front, where the rising CO emission indicates the transition into the molecular cloud (Tielens et al. 1993; van der Werf et al. 1996). These similarities suggest that all three arise from a common carrier or family of carriers. The spatial association of the excesses with the layers of H_2 and CO emission suggests that the existence of these simple molecules influences the composition of the PAHs.

4.1. *Hot Bands and Methyl Sidegroups*

Two models involving C—H stretching vibrations have previously been suggested to account for the 3.40 μm band: hot bands and molecular sidegroups. The 3.29 μm band arises from a $v = 1 \rightarrow 0$ transition in an aromatic C—H stretch. In the hot band model, the 3.40 μm band results from a $v = 2 \rightarrow 1$ transition (Barker, Allamandola, & Tielens 1987). Recent observations imply that the hot band explanation is unlikely. In some protoplanetary nebulae (PPNs), the strength of the 3.40 μm band approaches that of the 3.29 μm band (Geballe & van der Veen 1990; Geballe et al. 1992). Schutte, Tielens, & Allamandola (1993) show that the internal vibrational energies required to produce a hot-band–to–main-band ratio (3.40 μm/3.29 μm) of ≥ 0.17 would rupture the C—H bond. Furthermore, the observed intensity of the overtone ($v = 2 \rightarrow 0$) at 1.68 μm in IRAS 21282+5050 implies that the hot band occurs at 3.43 μm, not 3.40 μm, and that it is too weak to account for the bulk of the 3.40 μm band (Geballe et al. 1994).

In the sidegroup model, aliphatic sidegroups attached to the periphery of vibrationally excited PAH molecules produce the 3.40 μm band, and potentially other bands in the 3 μm region as well (Duley & Williams 1981; de Muizon et al. 1986; Geballe et al. 1989). Joblin (1992) measured the first infrared spectra of isolated gas-phase PAHs with aliphatic sidegroups. Joblin et al. (1996) subsequently showed that laboratory spectra of coronene with methyl sidegroups (—CH_3) provide a reasonable spectral match to the observed 3.40 μm feature. However, the laboratory sample peaks at 3.41 μm, slightly to the red of the 3.40 μm feature.

4.2. *H—PAHs and Methyl Sidegroups*

PAHs with extra hydrogen atoms attached to the carbon atoms on the periphery will have both aromatic and aliphatic attributes. For example, complete hydrogenation of benzene (C_6H_6) produces the aliphatic molecule cyclohexane (C_6H_{12}). The fundamental C—H stretching vibrational frequencies for a carbon atom with two attached hydrogen atoms will fall in the 3.4 μm region as these bonds are aliphatic in nature. Schutte et al. (1993) suggested this class of PAHs as possible contributors to the 3.40 μm feature. At that time, however, no spectrosopic data were available on isolated PAHs with extra hydrogen. Recently, Bernstein, Sandford, & Allamandola (1996, 1997), in a study of photochemical evolution of PAHs, have examined this class of molecules. Schutte et al. (1993) described them as superhydrogenated PAHs (SPAHs), but Bernstein et al. (1996) refer to them as H_n—PAHs, where n indicates the number of additional H atoms. We will refer to these molecules as H—PAHs.

Figure 8 compares the spectrum of the Orion Bar with the absorption spectrum of a sample H—PAH, hexahydropyrene (HHP, courtesy of Bernstein et al. 1996) and shows that this molecule provides a good match to our Orion Bar spectrum from 3.35 to 3.60 μm. In particular, the peak at 3.395 μm fits the main component of the 3.40 μm feature very well. In addition, this molecule provides a better fit than methyl coronene to the emission features at 3.46 and 3.51 μm. At other wavelengths, the laboratory spectrum of HHP shows no features stronger than the 3.40 μm band (Bernstein et al. 1997). The wavelengths of the bands observed in the limited number of laboratory spectra suggest that methyl sidegroups might produce the 3.405 μm component while H—PAHs might produce the stronger 3.395 μm component. However, only a few species of H—PAH molecules have been examined in the laboratory (Bernstein et al. 1996, 1997), and the wavelengths of the observed bands will depend on both the degree of hydrogenation and the shape of the PAH molecule.

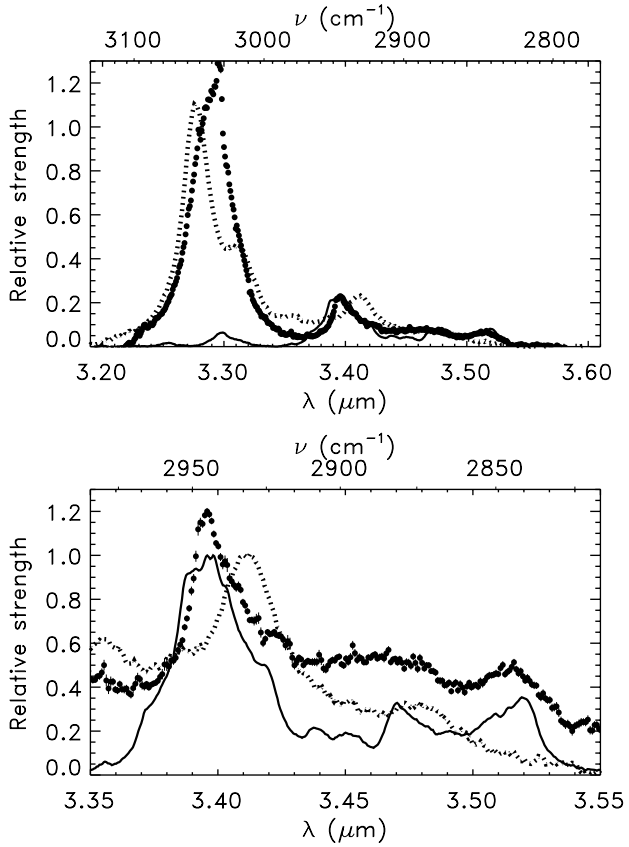

FIG. 8.—Spectrum from the Orion Bar (*filled circles*) compared to an H—PAH molecule (*solid line*; hexahydropyrene, courtesy of Bernstein et al. 1996), and methyl coronene (*broken line*, courtesy of Joblin et al. 1996). The Orion Bar spectrum is the sum of all rows from the ionized region to 4″ beyond the ionization front (rows 0–8, October 29 data). In the bottom panel, the Orion Bar spectrum has been offset vertically for clarity.

If the UV field is stripping methyl sidegroups and excess H—PAH hydrogen between the ionization front and the H_2 layer, then the assignment of the 3.395 μm component to H—PAHs and the 3.405 μm component to methyl sidegroups becomes more tenable. Because free atomic hydrogen is readily available in the region between the ionization front and the H_2 layer, H—PAHs can be created, destroyed, and recreated by H addition and abstraction reactions. However, due to the rarity of free methane and related molecules, once a methyl sidegroup has been stripped, it is

most likely gone for good. Thus, closer to the ionization front, the transition from molecular to atomic hydrogen would provide a chemical explanation of how the abundance of methyl sidegroups can be reduced while the H—PAH portion of the PAH population is maintained.

The 3.40 μm emission feature most likely arises from aliphatic C—H bonds. Whether this carbon resides within polycyclic structures (H—PAHs) or within methyl sidegroups and related linear chains, or both, remains unclear. The solution promises to be very important to understanding how carbon forms into PAHs and how carbon is processed in the interstellar medium.

5. CONCLUSION

The strong PAH band at 3.29 μm generally shows an exponentially decreasing intensity with increasing distance from the ionization front into the molecular region, with two regions of excess emission $\sim 10''$ and $\sim 20''$–$25''$ behind the ionization front. The main component of the 3.40 μm feature, the PAH plateau, and the 3.51 μm band all have very similar spatial distributions, with stronger and more extensive excesses $\sim 10''$ and $\sim 20''$–$25''$ behind the ionization front. The weaker 3.46 μm band shows no excesses at all; its spatial behavior is more consistent with an exponential falloff.

The similarity in the behavior of the main component of the 3.40 μm feature, the 3.51 μm band, and the PAH plateau suggests that they share a common origin. Whatever the precise nature of the carrier of the main component of the 3.40 μm band, this same carrier probably also produces the 3.51 μm band and the PAH plateau as well. The lack of correlation between the 3.46 μm band and the extra component of the 3.40 μm feature suggests that these two features arise from different carriers.

While we cannot identify individual molecular carriers of the observed spectral features, we can identify classes of molecules for which the laboratory spectra fit the astronomical spectra closely. The 3.29 μm band requires that the majority of the emitting material have an aromatic structure. The weaker bands in the 3 μm region may arise from aliphatic carbon associated with aromatic material. Two classes of molecules, H—PAHs and PAHs with methyl sidegroups, have aliphatic C—H stretches that may contribute to the 3.40 μm band.

More laboratory data on H—PAHs and methyl sidegroups would allow us to draw firmer conclusions, as would high-quality spectra of astronomical sources that have different physical conditions (such as reflection nebulae) or show very strong emission at 3.40 μm (such as PPNe).

We wish to thank the staff of the United Kingdom Infrared Telescope and the Joint Astronomy Centre for their excellent support. M. Bernstein and S. Sandford have very kindly provided us with some of their laboratory measurements and engaged us in many stimulating and useful discussions. C. Joblin made many useful comments on the manuscript and also provided us with laboratory data. The comments of the referee, L. d'Hendecourt, led to several improvements. G. C. S. is supported by the National Research Council as an Associate at NASA Ames Research Center, and during the reduction of these data was hosted by the Institute for Particle Physics and Astrophysics at Virginia Tech. C. E. W. acknowledges support of the National Science Foundation grant AST 94-53354.

REFERENCES

Allamandola, L. J., Tielens, A. G. G. M., & Barker, J. R. 1985, ApJ, 290, L25
———. 1989, ApJS, 71, 733
Barker, J. R., Allamandola, L. J., & Tielens, A. G. G. M. 1987, ApJ, 315, L61
Bernstein, M. P., Sandford, S. A., & Allamandola, L. J. 1996, ApJ, 472, L127
———. 1997, in preparation
Black, J. H., & van Dishoeck, E. F. 1987, ApJ, 322, 412
Blanco, A., Bussoletti, E., & Colangeli, L. 1988, ApJ, 334, 875
Borghesi, A., Bussoletti, E., & Colangeli, L. 1987, ApJ, 314, 422
Bregman, J. D., Allamandola, L. J., Tielens, A. G. G. M., Geballe, T. R., & Witteborn, F. C. 1989, ApJ, 344, 791
Bregman, J. D., Larson, K., Rank, D., & Temi, P. 1994, ApJ, 432, 326
Bregman, J. D., & Sloan, G. C. 1996, in From Stardust to Planetesimals: Contributed Papers, ed. M. E. Kress, A. G. G. M. Tielens, & Y. Pendleton, in press
de Muizon, M., Geballe, T. R., d'Hendecourt, L. B., & Baas, F. 1986, ApJ, 306, L105
Duley, W. W., & Williams, D. A. 1981, MNRAS, 196, 269
Geballe, T. R., Joblin, C., d'Hendecourt, L. B., Jourdain de Muizon, M., Tielens, A. G. G. M., & Léger, A. 1994, ApJ, 434, L15
Geballe, T. R., Lacy, J. H., Persson, S. E., McGregor, P. J., & Soifer, B. T. 1985, ApJ, 292, 500
Geballe, T. R., Tielens, A. G. G. M., Allamandola, L. J., Moorhouse, A., & Brand, P. W. J. L. 1989, ApJ, 341, 278
Geballe, T. R., Tielens, A. G. G. M., Kwok, S., & Hrivnak, B. 1992, ApJ, 387, L89
Geballe, T. R., & van der Veen, W. E. C. J. 1990, A&A, 235, L9
Gillett, F. J., Forrest, W. J., & Merrill, K. M. 1973, ApJ, 183, 87
Grasdalen, G. L., & Joyce, R. R. 1976, ApJ, 205, L11
Joblin, C. 1992, Ph.D. thesis, Université Paris
Joblin, C., Tielens, A. G. G. M., Allamandola, L. J., & Geballe, T. R. 1996, ApJ, 458, 610
Jones, A. P., Duley, W. W., & Williams, D. A. 1990, QJRAS, 31, 567
Léger, A., d'Hendecourt, L. B., & Défourneau, D. 1989, A&A, 216, 148
Léger, A., & Puget, J. L. 1984, A&A, 137, L5
Merrill, K. M., Soifer, B. T., & Russell, R. W. 1975, ApJ, 200, L37
Papoular, R., Conard, J., Guiliano, M., Kister, J., & Mille, G. 1989, A&A, 217, 204
Sakata, A., Wada, S., Onaka, T., & Tokunaga, A. 1987, ApJ, 320, L63
Schutte, W. A., Tielens, A. G. G. M., & Allamandola, L. J. 1993, ApJ, 415, 397
Sellgren, K. 1981, ApJ, 245, 138
———. 1984, ApJ, 277, 623
Tielens, A. G. G. M., Meixner, M. M., van der Werf, P. P., Bregman, J., Tauber, J. A., Stutzki, J., & Rank, D. 1993, Science, 262, 86
van der Werf, P. P., Stutszki, J., Sternberg, A., & Krabbe, A. 1996, A&A, submitted